Modeled Response of South American Climate to Three Decades of Deforestation

Yelin Jiang[a], Guiling Wang[a]*, Weiguang Liu[a,b], Amir Erfanian[a], Qing Peng[b], Rong Fu[c]

[a]Department of Civil and Environmental Engineering and Center for Environmental Sciences and Engineering, University of Connecticut, Storrs, CT, USA

[b]Key Laboratory of Meteorological Disaster of Ministry of Education, and International Joint Laboratory on Climate and Environment Change, Nanjing University of Information Science and Technology, Nanjing, China

[3]Joint Institute for Regional Earth System Science and Engineering, Department of Atmospheric and Oceanic Sciences, University of California, Los Angeles, CA, USA

* Correspondence: guiling.wang@uconn.edu; 860 486 5648

Abstract

This study investigates the potential effects of historical deforestation in South America using a regional climate model driven with reanalysis data. Two different sources of data were used to quantify deforestation during 1980-2010s, leading to two scenarios of forest loss, smaller but spatially continuous in Scenario 1 and larger but spatially scattered in Scenario 2. The model simulates a generally warmer and drier local climate following deforestation. Vegetation canopy becomes warmer due to reduced canopy evapotranspiration, and ground becomes warmer due to more radiation reaching the ground. The warming signal for surface air is weaker than for ground and vegetation, likely due to reduced surface roughness suppressing the sensible heat flux. For surface air over deforested areas, the warming signal is stronger for the nighttime minimum temperature and weaker or even becomes a cooling signal for the daytime maximum temperature, due to the strong radiative effects of albedo at midday, which reduces the diurnal amplitude. The drying signals over deforested areas include lower atmospheric humidity, less precipitation, and drier soil. The model identifies the La Plata basin as a region remotely influenced by deforestation, where a simulated increase of precipitation leads to wetter soil, higher ET, and a strong surface cooling. Over both deforested and remote areas, the deforestation-induced surface climate changes are much stronger in Scenario 2 than Scenario 1; coarse resolution data and models (such as in Scenarios 1) cannot represent the detailed spatial structure of deforestation and underestimate its impact on local and regional climates.

1. Introduction

The Amazon rainforest is one of the largest carbon pools on Earth, which stores approximately 150-200 Pg C in living biomass and soils (Feldpausch et al., 2012), and plays a crucial role in the regional and global water, energy, and carbon cycles (Houghton et al., 2000; Brienen et al., 2015; Cavalcante et al., 2019). However, more than 20% of Amazon forest has been replaced by pasture and cropland since the early 1970s (Fearnside, 2005; Davidson et al., 2012; Souza-Filho et al., 2016). After decades of severe deforestation, the rate of forest loss slowed down between 2004 and 2012, mostly due to Forest Code changes in Brazil (Soares-Filho et al., 2014; Alves et al., 2017; Rochedo et al., 2018). However, since 2012, the deforestation rate has picked up again due to relaxed policy and accelerated agricultural development, putting the Amazon ecosystem at risk (Tollefson, 2016). For example, the annual deforestation area decreased from 19000 km^2 in 2005 to 4500 km^2 in 2012, and rebounded to 5900 km^2 in 2013 (Prodes, 2013).

Land cover change modifies the surface water and energy budgets through several mechanisms (Swann et al., 2015; Wang et al. 2016b). Converting forest to cropland and grassland increases surface albedo, which tends to cool the surface through reduced absorption of solar radiation. On the other hand, the reduction of leaf area and canopy interception, as well as the loss of moisture-tapping deep roots in the dry season, all contribute to reducing evapotranspiration, which tends to increase surface temperature. In addition, deforestation-induced decrease of surface roughness reduces the turbulent transport of heat to atmosphere, which also induces a surface warming effect (Lejeune et al., 2015).

There is a high degree of consensus among previous modeling studies that deforestation in the Tropics leads to higher temperature, as the loss of evaporative cooling is dominant over the radiative effect of albedo changes (Lean & Warrilow, 1989; Malhi et al., 2008; Swann et al., 2015). Taking a space-for-time approach, many observational studies found a warming effect of deforestation by comparing temperature between cleared land and nearby forests (e.g., Duveiller et al. 2018; Cohn et al. 2019) with a stronger signal during daytime than at night (e.g., Li et al. 2015; Alkama and Cescatti 2016; Schultz et al. 2017). The asymmetric effects (and therefore the amplification of temperature diurnal cycle) found in observational studies may be partly due to the space-for-time approach not being able to account for the cloud effects related to atmospheric feedback (Chen and Dirmeyer 2020). A notable recent study (Zeppetello et al. 2020) analyzed daytime temperature from satellite observations in areas that were forest in 2003 and open land in 2018 and found a significant warming signal that increases with the size of the deforestation patch.

The impact of deforestation is not limited to the surface. Evapotranspiration is an important source of moisture supply for precipitation in the Amazon Basin, accounting for 15-50% of total Amazonian rainfall (Zemp et al. 2017; Van der Ent et al. 2010; Eltahir and Bras 1994; Satyamurty et al. 2013). The deforestation-induced reduction of evapotranspiration in the dry season can weaken regional atmospheric moisture recycling and reduce precipitation, which may trigger a positive vegetation-precipitation feedback that could drive forest loss in regions where the local climate approaches the water and temperature thresholds of existing vegetation (Da Rocha et al. 2009; Van der Ent et al. 2010;

Wang et al., 2011; Zemp et al. 2017).

The impact of deforestation on precipitation is subject to a large degree of uncertainty and depends on the scale and location of the forest loss. Most modeling studies on idealized large-scale deforestation in the Amazon region found a decrease of precipitation (e.g., Lean & Warrilow, 1989; Gedney & Valdes, 2000; Nobre & Borma, 2009; Sampaio et al., 2007). However, small-scale patches of deforestation that are common in tropical rainforests could increase cloudiness and precipitation through thermally induced mesoscale circulations (Baidya Roy & Avissar, 2002; Wang et al., 2009; Lawrence & Vandecar, 2015; Khanna et al., 2017). As the spatial extent of deforestation increases beyond a certain level, the thermal triggering may weaken and shift to a dynamically driven hydroclimate regime, leading to an enhancement of convection in the downwind region and a suppression of convection in the upwind region (Patton et al., 2005). Khanna et al. (2017) suggested that the extent of Amazon deforestation may have crossed the threshold for the thermal-to-dynamic transition of the hydroclimate regime.

Monitoring the magnitude of deforestation in the Amazon is challenging, due to difficulties in identifying temporal thresholds and spatial scales, integrating field and satellite datasets, as well as evaluating spatial impact and intensity (Herold et al., 2011). Quantifying the extent of historical deforestation involves further challenges. Skole & Tucker (1993) estimated deforestation over the Brazilian Amazon Basin from 1978 to 1988 through Landsat satellite data of 1978 and 1988. Since the launch of the Moderate Resolution Imaging

Spectroradiometer (MODIS) in 2000, it has been widely used as the main approach to vegetation remote sensing in the Amazon (Huete et al., 2002). MODIS-derived deforestation was verified through comparison with Landsat-derived deforestation estimates (Morton et al., 2005) and annual deforestation data derived from the Amazon Deforestation Monitoring Project (PRODES) (Hansen et al., 2008). Hilker et al. (2015) measured changes of Amazon vegetation using MODIS Enhanced Vegetation Index (EVI) and Normalized Difference Vegetation Index (NDVI) between 2000 and 2012. However, as remote sensing cannot capture the loss of biomass until it interrupts the canopy continuity (e.g., selective logging), it may underestimate the severity and extent of deforestation (Milodowski et al. 2017).

The goals of this study are to quantify the impact of historical land cover changes of realistic magnitude on regional climate of Amazon during 1980s-2010s, investigate the different mechanisms and processes in different regions and seasons, and assess how the climatic effects of land cover changes depend on the source and nature of land cover change data. For these purposes, we employ a regional climate model with sophisticated representation of land surface processes and impose to the model deforestation scenarios constructed from observational data and simulated data. Section 2 describes the model, data, and experimental design. The results are presented in Section 3, followed by a summary and discussion in Section 4.

2. Model, Data, and Experimental Design

This study makes use of the International Center for Theoretical Physics (ICTP) Regional Climate Model version 4.3.4 (RegCM4.3.4, Giorgi et al., 2012) coupled with the Community Land Model version 4.5 (CLM4.5, Oleson et al., 2013) (RCM-CLM, Wang et al., 2016a). In this coupled land-atmosphere system model, RCM simulates the atmospheric dynamical and physical processes, while CLM simulates the land surface hydrological, biogeophysical and biogeochemical processes, plant phenology, and vegetation dynamics. CLM solves the water and energy fluxes at the level of plant functional types (PFTs), and grid-level fluxes (and properties such as leaf area index (LAI) and albedo) are area-weighted averages among the different PFTs. While the model has the capacity to simulate vegetation dynamics, in this study we prescribe vegetation conditions (structure, distribution, and phenology) to be static. That is, the LAI of each PFT varies from day to day but the LAI seasonal cycles and PFT coverages remain the same from year to year. The model performance was validated for Africa, Asia and South America (Yu et al. 2016; Wang et al. 2016a; Erfanian et al. 2017b; Shi et al. 2018; Liu et al. 2020a,b). Specifically for South America, Erfanian & Wang (2018) conducted experiments on multiple domain sizes and locations, and found that the model performance improves when the domain expands beyond the Coordinated Regional Downscaling Experiment (CORDEX) domain to include the influential oceans. In this study, we follow the Erfanian & Wang (2018) approach in adopting a domain that spans the region 152° W-12° E, 56° S-44° N including South America, a major portion of North America and the Pacific and Atlantic Oceans.

We investigate how deforestation during 1980s-2010s may have influenced regional climate based on RCM-CLM simulations that differ in vegetation cover in South America. The lateral boundary conditions (LBCs) for all simulations are derived from the 6-hourly 1.5° resolution ERA-Interim data (Dee et al., 2011). Two different sources of deforestation data were used to derive three sets of land covers, using the spatial coverage of each PFT from the Moderate Resolution Imaging Spectroradiometer (MODIS) remote sensing data corresponding to year 2000 (Lawrence et al., 2011; Lawrence & Chase, 2007) as a medium (referred to as "Land_2000" hereafter). We derived the PFT spatial coverages for "Land_1980" and "Land_2015" by combining the "Land_2000" MODIS data with forest cover changes from the land use harmonization (LUH2) dataset (Hurtt et al., 2011) during 1980-2000 (for "Land_1980") and 2000-2015 (for "Land_2015"), respectively (Figure 1a1), and derived the PFT spatial coverages for "Land_2017" by combining the "Land_2000" MODIS data with forest cover changes derived from Landsat data during 2000-2017 (Hansen et al., 2013) (Figure 1a2). Imbach et al. (2015) indicated that for most countries in the Amazon basin the ratio of pastureland area to cropland area is typically 4:1. Thus, in this study, deforested areas were converted to 20% cropland and 80% pasture. Note that the LUH2 data is at 0.5°×0.5° resolution, and was linearly interpolated to the RCM resolution of 50km×50km; Landsat data is at 30m×30m resolution, and was aggregated to the RCM resolution through arithmetic averaging among all pixels within each RCM grid. So the derived land cover data "Land_1980" and "Land_2015" are coarse resolution representation of vegetation state in the early 1980s and in mid-2010s, respectively, while "Land_2017" partially retains the spatial structure of vegetation cover in mid-2010s. We are making these derived land cover data available through GitHub (https://github.com/Yelin-Jiang/land_cover_data_JCLI-D-20-0380).

The three different land cover datasets were then used to prescribe vegetation for three RegCM-CLM experiments, “Land_1980”, “Land_2015”, and “Land_2017”, named after their corresponding land cover data respectively. The atmospheric model in all three experiments was driven with the same atmospheric boundary conditions during the period 1996-2017 to simulate climate of the past two decades corresponding to three different land cover scenarios; in each experiment, the coverage of each PFT and its LAI seasonal cycle do not vary from year to year. This sensitivity experimental design allows us to assess how vegetation changes during 1980s-2010s might influence the regional climate using the period 1996-2017 as an example. The three simulated climates represent hypothetically how the climate during 1996-2017 would be if the vegetation were the same as described by Land_1980, Land_2015, and Land_2017 datasets, respectively. The simulated climate differences between Land_1980 and Land_2015 (Scenario 1) can quantify the effects of coarse-resolution land cover changes on regional climate; differences between Land_1980 and Land_2017 (Scenario 2) account for the impact of a more realistic spatial structure of deforestation and provide an alternative for comparison with Scenario 1 results. The two scenarios were used to assess how the climatic effects of land cover changes may depend on the spatial structure of land use/land cover changes.

For more detailed results analysis, we selected 9 severely deforested areas of 3°×3° in size from three regions: cluster 1 includes areas 1, 2 and 3 in the South Amazon (SouA), cluster 2 includes areas 4, 5 and 6 in the Brazilian Highlands (BRH), and cluster_3 includes areas 7, 8 and 9 in the East Amazon region (EastA). The same selected boxes of Scenario 1 and Scenario 2 are shown in Figure 1. The SouA and EastA are wet regions with a five-month wet season, and BRH is a dry region with a three-month wet season. Here wet season is defined as the period when daily precipitation exceeds 6.1 mm/day, following the method of Li & Fu (2004). In Land_1980, the simulated annual average of daily precipitation is 5.28 mm/day, 3.26 mm/day and 5.22 mm/day for the SouA, BRH and EastA, respectively. Over the region as a whole, the total area of forest cover loss is 837 million ha in Scenario 1 and 731 million ha in Scenario 2; over the three clusters of severe forest loss, the lost forest cover as a percentage of total land area is 20.57%, 21.99% and 12.11% for the SouA, BRH and EastA clusters in Scenario 1, and is 21.90%, 15.03% and 18.18% in Scenario 2, respectively. However, due to the high degree of spatial heterogeneity of forest loss and substantially different spatial pattern, greater difference between the two scenarios can be found in the magnitude of forest loss over some localized areas (Figures 1a1-1a2). For example, for Region 8 within EastA, the forest cover loss averages to 22.35% in Scenario 2 and only 7.95% in Scenario 1.

3. Results

3.1 Surface biogeophysical properties

Deforestation influences regional climate through not only the release of greenhouse gases but also the shifts in surface biogeophysical properties (Houspanossian et al., 2017). LAI is expected to decrease as the land cover is converted from forest to cropland and grassland. Figures 1b1 and 1b2 show the derived LAI changes over deforestation regions in Scenario 1 and Scenario 2. The LAI changes in Scenario 1 are modest in magnitude and spatially continuous, although there are some spots of relatively large changes in SouA; the LAI changes in Scenario 2 tend to be larger in magnitude but spatially concentrated over small fragmented areas, with most pixels of largest LAI changes found in SouA and EastA. These differences result partly from the very different spatial resolution of the raw data from which these changes were derived. In Scenario 1, LUH2 simulated data (1980-2015) is at 0.5°×0.5° spatial resolution; for Scenario 2, land cover change is influenced by both the LUH2 simulated data (1980-2000) and the 30m×30m Landsat observational data (2000-2017). In addition to LAI changes, changes from dark forests to bright cropland and grassland lead to higher surface albedo (Figures 1c1-1c2). The increase of albedo shows spatial correspondence to land cover changes of the corresponding scenario, but the magnitude of the increases is small and mostly less than 0.01. Another important aspect of deforestation is the reduction in surface roughness, which increases wind speed (Figure S1) but may reduce turbulence therefore surface heat fluxes. These changes to the surface biogeophysical properties influence local and regional climate through their impact on the surface water and energy budgets.

3.2 Impact on the Terrestrial Water Cycle

The loss of forest cover directly influences the terrestrial hydrological cycle (Table 1). Evapotranspiration (ET) includes contributions from evaporation of precipitation intercepted by the vegetation canopy (E_c), plant transpiration (T_r), and ground evaporation (E_g) from the soil surface. The responses of ET and its components to deforestation are highly consistent among different seasons, with a common spatial pattern across all seasons (results not shown), so only the annual average responses are shown in Figure 2. Over most deforested areas in Amazon, the decrease of leaf area reduces canopy evaporation and transpiration; another cause for the decrease of T_r has to do with the loss of deep tree roots that tap moisture from deep soil during the dry season or in dry regions. However, E_g is simulated to increase following deforestation (Figure 2), as the removal of tree canopy allows more solar radiation to reach the ground, warming the soil and driving up the ground evaporation. This is especially the case in wet regions (SouA and EastA) or wet seasons when energy input into the land surface (as opposed to soil water availability) is the primary limiting factor for E_g. Therefore, the net effects of deforestation on ET (sum of E_c, T_r, and E_g) is relatively small, especially for Scenario 1. For each ET component and the total ET, the changes in Scenario 2 are larger in magnitude than in Scenario 1 and show a clearer spatial correspondence with land cover changes (Figure 2).

The ET changes and the corresponding component changes as shown in Figure 2 have to do with whether the ET regime is energy-limited or water-limited. In the wet regions (or wet seasons), energy availability and area of the transpiring surface plays a dominant role in the ET changes. The annual average reduction in ET in SouA and EastA are -0.006 mm/day and -0.004 mm/day in Scenario 1 and -0.015 mm/day and -0.022 mm/day in Scenario 2 (Table 1). In the drier region BRH, water availability dominates the change of ET in most seasons. The annual average changes in BRH feature an increase in ET and are similar between the two scenarios, both with an approximate increase of 0.05 mm/day, a result of increased precipitation related to large scale precipitation changes.

In SouA and EastA, E_c decreases in wet seasons as a result of deforestation-induced leaf area reduction but shows little signal in the dry season (June, July, and August, “JJA” hereafter) due to the lack of precipitation (therefore lack of canopy interception) (results not shown). For the same reason, simulated E_c changes are negligible during most seasons in the BRH region when precipitation is absent and features a slight increase in the wet season due to a large-scale increase of precipitation in that region simulated by the model. The response of T_r and its spatiotemporal variability are qualitatively similar to E_c, with a decrease in wet regimes (e.g., SouA and EastA) and a precipitation-induced increase in BRH. In contrast, the response of E_g shows a high degree of spatiotemporal coherency, increasing across the deforested areas and during all seasons.

Deforestation causes a clear decrease of the near-surface relative humidity in the model within the deforested areas (Figure 3), which results from not only the reduced moisture supply through canopy evaporation and transpiration but also surface warming (as shown in section 3.3). This drying signal also extends to the lower troposphere over both deforested land and nearby areas, especially during the SON (September, October, and November, “SON” hereafter) season (Figure 3), leading to an overall decrease of cloudiness and suppressed precipitation (Figure 4). The precipitation response is the strongest in the SON season, with a clear decrease of precipitation over deforested areas; the precipitation signal in other seasons is weaker and mixed, leading to an overall weak signal in the annual average, although there is still a clear correspondence with the deforestation pattern (Figure 4). The lack of strong rainfall response during the wet season (December-May, results not shown) is expected, as a large part of moisture source is from transport by the monsoon circulation. During the dry season (JJA, results not shown), rainfall in most of Amazonia is already very low, leaving little room for further reduction. Over the deforested southern Amazonia during the pre-monsoon season (SON), ET is the primary moisture source for precipitation, so the simulated reduction of precipitation following deforestation is expected, as also shown by observational studies (e.g., Leite-Filho et al., 2019). Among the heavily deforested wet regions, the deforestation-induced change of annual precipitation averages to -1.41% over SouA and -1.06% over EastA in Scenario 1, and -1.65% over SouA and -3.95% over EastA in Scenario 2. In the drier region BRH, the annual average precipitation change is simulated to decrease in Scenario 1 (by -5.46%) and increase (by 3.18%) in Scenario 2. However, these precipitation signals are weak and do not pass the significance test over most grid cells of South America.

Precipitation is influenced by both local and non-local land cover changes (Hirota et al., 2011), through both moisture supply and circulation changes. Through moisture supply, deforestation influences atmospheric humidity and precipitation in the deforested areas and downwind. Additional remote impact can occur through large-scale circulation changes. In the subtropics over the La Plata basin with little or no local deforestation, a notable increase of precipitation is simulated during most seasons and in the annual average (Figure 4), apparently a result of large circulation changes associated with non-local deforestation. This increased precipitation is the primary cause for the increase of evapotranspiration and soil moisture in the La Plata basin (Figure 2 and Figure 4), a dry region where ET is limited by water availability.

Over deforested region, soil moisture features a clear drying signal, as shown in Figure 4 using moisture in the top 10cm of the soil (W_{soil}) as an example; the response in deeper soils is qualitatively similar. In the wet regions, SouA and EastA, the spatially averaged, annual mean W_{soil} change is -0.299 mm and -0.114 mm for Scenario 1 and -0.279 mm and -0.421 mm for Scenario 2 in the top 10cm of soil (Table 1). This decrease of soil moisture results from the combination of a slight decrease of precipitation (especially in South Amazon) and a broad increase of evaporation from the soil surface, and suggest that land cover change may have contributed to the severe depletion of terrestrial water storage found in South Amazon and EastA regions during recent droughts (Erfanian, et al., 2017a). In the drier region BRH, the response of W_{soil} in the model is inconclusive, with a slight decrease in Scenario 1 and slight increase in Scenario 2, consistent with precipitation responses.

As the deforested areas are spatially scattered across a large region, spatial averages (e.g., Tables 1) do not reflect the true magnitude of the local response at the grid cell level. Figure 5 relates the deforestation-induced water cycle changes in each model grid cell to the magnitude of local forest cover loss, and includes all grid cells in the Amazon where deforestation exists. The magnitude of water cycle responses (including increase of E_g and decreases of E_c, T_r, ET, precipitation, and soil moisture) generally increases with the extent of deforestation within each grid, although the range of uncertainty is quite large. For a given magnitude of forest cover loss, the hydrological response does not differ qualitatively between the two scenarios; differences between the two scenarios in the simulated water cycle responses (Figure 2) are primarily attributed to the magnitude of forest cover loss applied to the model. Specifically, forest cover loss in Scenario 1 is less than 40% in most grid cells; for all grid cells with less than 40% forest cover loss in Scenario 2, the water cycle changes derived from the Scenario 2 experiment are similar to those derived from Scenario 1 (Figure 5), although E_c, T_r, and E_g show stronger responses in Scenario 2 at some grid cells. The large magnitude of water cycle changes found in Scenario 2 result primarily from forest loss that are larger in magnitude (more than 40%) despite being spatially fragmented. Among the grid cells approaching complete forest loss, the average decrease of ET and precipitation is approximately 0.5 and 0.75 mm/day, respectively. The clear contrast between the two scenarios has significant implications. Although deforestation often occurs in the form of severe forest loss concentrated over fragmented areas (as shown by Scenario 2), coarse-resolution data and climate models often represent deforestation as land cover changes of small magnitude over spatially continuous and extensive areas (as shown by Scenario 1) and thus underestimate the local climatic impact of deforestation.

3.3 Impact on Surface Temperature and Energy Budget

Consistent with previous studies, results from the three experiments indicate that deforestation leads to higher surface temperature (Table 2). Vegetation temperature (T_v) increases markedly across the deforested areas, which results from the decrease of E_c and T_r; meanwhile, ground temperature (T_g) increases over the deforested areas as a result of more solar radiation reaching the ground following the reduction of LAI (Figure 6). The spatial pattern of T_v and T_g responses feature a clear signal that is spatially continuous in Scenario 1 and scattered in Scenario 2, similar to the corresponding forest cover loss for the two scenarios. The deforestation-induced increase of annual average T_v is approximately 0.30 °C in SouA for both scenarios, and is 0.16 °C in Scenario 1 and negligible (0.02 °C) in Scenario 2 when averaged over BRH. In EastA, the annual T_v warming is 0.16 °C for Scenario 1 and 0.33 °C for Scenario 2. Compared to vegetation temperature, ground temperature shows a greater sensitivity to the loss of forest cover. Averaged over the SouA, BRH and EastA regions respectively, the changes of annual mean T_g are 0.59 °C, 0.38 °C, and 0.33 °C under deforestation Scenario 1 and 0.65 °C, 0.18 °C and 0.65 °C under Scenario 2. Warmer vegetation and warmer ground lead to an increase of the near surface air temperature (T_{2m}) along the arc of deforestation (Figure 6), with a smaller magnitude of warming in T_{2m} than in T_v and T_g. For the response of average temperature (including T_v, T_g, and T_{2m}) to deforestation, the spatial pattern is consistent among different seasons, with the largest magnitude of warming in the pre-monsoon season (SON). In the subtropics, consistent with the increased precipitation related to large scale circulation changes, temperature decreases as a result of both increased cloudiness and increased evapotranspiration.

The daily minimum 2m temperature (T_{2m_min}) (Figure 7) is simulated to increase, and the response is consistent across all seasons; the T_{2m_min} warming shows a similar spatial pattern to the average T_{2m} warming but is larger in magnitude. In contrast, the daily maximum 2m temperature (T_{2m_max}) is simulated to slightly increase or even decrease, and the cooling is stronger in Scenario 2 than in Scenario 1 and over both deforested and non-deforested areas (Figures 7-8, Table 2); the strongest cooling is simulated in the subtropics with little or no deforestation. The responses of the minimum, average, and maximum temperature at the lowest level of the atmosphere (results not shown) are similar to those of the 2m air temperature. Note that the decrease of the day-time maximum air temperature over deforested areas found here contradicts a strong warming signal found in observational studies that were mostly based on a “space-for-time” approach. Three factors contributed to the cooling signal simulated by our model. First, temperature response to deforestation depends heavily on the competition between the ET effects and albedo effects, and the cooling effects of albedo increase are the strongest during mid-day hours when the solar radiation is the strongest. Second, deforestation induces a large-scale circulation change with increased mid-day cloudiness and decrease of solar insolation, an effect that cannot be captured by the space-for-time approach in observational studies. Third, converting forest to cropland and grassland reduces surface roughness and efficiency of surface heat dissipation into the atmosphere (Chen and Dirmeyer 2019), leading to cooler air over a warmer ground.

Despite locally strong signals, spatially averaged air temperature changes are quite small in magnitude. For example, the warming of annual average T_{min} in SouA, BRH, and EastA regions are 0.38 °C, 0.30 °C, and 0.20 °C in Scenario 1 and 0.39 °C, 0.13 °C, and 0.37 °C in Scenario 2 (Table 2). At the grid-cell level, the changes in surface temperature generally scale with the magnitude of local tree cover loss (Figure 8a). For example, the coefficient of spatial correlation between annual average T_{2m} change and forest cover loss is 0.67 in Scenario 1 and 0.80 in Scenario 2. The approximately linear relationship seems to hold as forest cover loss continues to increase, and the simulated warming signal reaches 2-3°C in areas of complete forest loss. The relationship as shown in Figure 8a, together with the good correspondence between spatial patterns of deforestation and temperature response, indicates that surface temperature response is dominated by local effect in the Amazonia. The cloud-moderated effects (through incident shortwave radiation, "SW" hereafter) on temperature in deforested areas is also analyzed (Figure 8b), and the correlation coefficient between annual average T_{2m} change and SW change is 0.59 in Scenario 1 and 0.56 in Scenario 2. Note that this correlation results from complex feedback processes involving not only the warming effect of solar radiation but also the contribution of warming to reduced relative humidity therefore reduced cloudiness. In areas surrounding deforestation, a stronger correlation is found between the average T_{2m} change and SW change, with a correlation coefficient of 0.79 in Scenario 1 and 0.84 in Scenario 2 (Figure 8c), which reflect the non-local effect of deforestation. However, within the Amazon region, the magnitude of the non-local effects is relatively small (Figure 8c). At grid points where SW increases, the warming of daily average temperature is less than 0.3°C in grid cells with no deforestation (Figure 8c), and can be one order of magnitude higher in some grid cells with severe deforestation (Figure 8b). This contrast between Figure 8b and 8c indicates that the large magnitude of warming over deforested areas results primarily from local processes, with SW changes playing a secondary role. In contrast, the relationship between T_{2m_max} and SW for deforested grid cells is generally similar to the relationship for grid cells with no forest loss (Figure 8e vs. 8f), which indicates that cloud feedback related to large-scale circulation changes play an important role in the response of day-time maximum temperature to deforestation.

The effects of deforestation on surface energy budget are estimated based on their annual averages (Figure 9). Over deforested areas, surface insolation (SW) increases as a result of fewer clouds, but the net shortwave absorption is smaller due to the increase of surface albedo. The surface longwave emission (LW) increases as a result of warmer vegetation and warmer ground in the Tropics (Figure 9b1-9b2); in the subtropics, LW features a decreasing signal owing to the decrease of surface temperature caused by non-local deforestation. The net radiation changes are dominated by longwave emission response, with a general decrease over deforested areas, and are larger for Scenario 2 than Scenario 1 (Figure 9c1-9c2). With the general decrease of total ET following deforestation, latent heat flux (LE) decreases over most of the heavily deforested areas (Figure 9d1-9d2), but the signal is much weaker than the net radiation decrease (Figure 9c1-9c2). As a result, sensible heat flux (SH) decreases substantially (Figure 9e1-9e2). At the process level, converting forest to cropland and grassland reduces surface roughness and the turbulent transport of heat to the overlying atmosphere. This, together with the general decrease of R_{net}, causes a decrease of sensible heat flux over deforested areas.

The general warming over deforested areas may influence temperature extremes. The 99th percentile of daily average temperature (T_{99}) is enhanced over deforested areas in SouA and EastA, but is reduced in BRH (Figure 10). Averaged over the three deforestation clusters, the changes of T_{99} in Scenario 2 (0.33 °C, -0.38 °C, and 0.33 °C respectively) are larger than in Scenarios 1 (0.19 °C, -0.06 °C, and 0.13 °C respectively for SouA, BRH, and EastA). Similar to T_{99}, the extreme temperature frequency (F_{T99}, number of days with T_{2m} exceeding T_{99} from the Land_1980 experiment) increases in SouA and EastA but decreases in BRH (Figure 10). In Scenario 2, F_{T99} increases substantially, by 3.91 days/year in EastA (which means the frequency more than doubles its pre-deforestation value), and by 2.72 days/year in SouA. Note that SouA and EastA are wet regions with a high ET rate in Land_1980, while BRH is a dry region with a water-limited ET regime. Changes in both the intensity and frequency of the extreme temperature are larger for Scenario 2 than Scenario 1, indicating that coarse resolution, spatially continuous representation of deforestation tends to cause underestimation of the extreme temperature events in the model.

4. Conclusions and Discussion

In this paper, we derive two scenarios of deforestation-induced land cover changes in

South America during 1980s-2010s from two different sources of data, and assess how these changes might influence the regional climate. Converting forest to cropland and grassland leads to lower LAI and surface roughness and higher surface albedo. As a result of these deforestation-induced surface property changes, the model's surface climate becomes generally warmer and drier over deforested areas in the tropics. The surface warming signal is stronger for the ground and vegetation temperatures, and weaker for air temperature; for the surface air temperature, the warming signal is stronger for the nighttime minimum and weaker or even becomes a cooling signal for the daytime maximum temperature, which reduces the diurnal amplitude of air temperature over deforested areas. The surface drying signals include lower atmospheric humidity, less precipitation, and drier soil over deforested areas.

In addition to the local effects, deforestation causes non-local effects through altering atmospheric circulation and therefore moisture transport (Badger and Dirmeyer, 2016; Hasler et al., 2009). In the subtropics of South America including part of the La Plata basin where no land cover changes were imposed in the model, an increase of precipitation is simulated, apparently as a result of large-scale circulation changes associated with deforestation in the Amazon and surrounding regions. The increased precipitation leads to wetter soil, higher evapotranspiration, and a strong cooling signal in all temperatures examined.

The simulated temperature and water cycle changes resulting from deforestation show substantial differences between the two scenarios of deforestation. Coarse resolution data (as used in Scenario 1) underestimates the severity of forest loss at the grid cell level, which causes the model to underestimate the local impact of deforestation. In Scenario 1, the grid-level forest cover loss rarely exceeds 40%, and the projected local warming is mostly less than 1°C; in Scenario 2, the model suggests a warming of close to 3°C for grid cells with complete forest loss. The differences between the two scenarios in the simulated warming effects confirm the findings from recent studies (Khanna et al., 2017; Zeppetello et al., 2020) that the deforestation-induced hydrothermal changes are closely related to the deforested patch size. It is important that data and models used to study deforestation be able to capture the detailed spatial structure of land use land cover changes.

The cooling or weak warming of daytime maximum and the reduced diurnal amplitude of surface air temperature as a response to deforestation seem to contradict findings from observation-based studies that documented a significantly higher daytime temperature over open land than the neighboring forest areas. Several factors contribute to this discrepancy. From the model side, some simulated responses, especially the comparison among competing mechanisms, may be model specific. In this particular model, the evapotranspiration response is rather modest. During midday when the incoming solar radiation is the strongest, the radiative effects of albedo increase and the cloud effects related to a circulation change may outcompete the evapotranspiration effects. Meanwhile, reduced surface roughness suppresses latent heat flux, which may cause cooler air over a warmer ground. From the observation side, most studies relied on satellite-sensed temperature differences between forest and nearby patches of open land, which reflect the differences in ground temperature (as opposed to air temperature), and the “space for time” approach cannot capture the atmospheric feedback effect that is important for the simulated air temperature response in the model (e.g., Chen and Dirmeyer, 2020). This discrepancy will be the subject of our follow-up research.

Our study identifies the subtropical South America as a region remotely influenced by deforestation in the Amazon and surrounding regions. Observational data indicates that the La Plata basin has experienced increased precipitation and flooding in recent decades, accompanied by relatively slow warming trend or even cooling in some areas (e.g., Barros et al., 2015). Our model simulates similar signals, as a response to non-local deforestation, including an increased precipitation resulting from altered large-scale circulation and a strong cooling due to the associated cloud effects as well as enhanced surface evapotranspiration under increased water availability. These results suggest that non-local deforestation may have contributed to the observed climate trends in the La Plata basin.

For all temperature indicators evaluated in this study, the strongest warming signal is simulated in SON, the dry-to-wet transition season; SON is also the most sensitive season in terms of precipitation response. This is consistent with the argument put forward by Fu & Li (2004) and Li & Fu (2004). Specifically, the interactions between rainfall and large-scale, low-level convergence, as well as higher surface wetness during the wet seasons (DJF and MAM) tend to self-amplify and self-sustain the conditions favorable for rainfall until the seasonal maximum solar radiation moves away from this region; on the other hand, the dry-to-wet transition during SON has to overcome the surface dryness and inversion at the top of the boundary layer, which in the absence of summer large-scale circulation may depend more on land surface processes.

Other than anthropogenic land use changes, self-amplified forest loss may result from the interactions between vegetation and regional climate (Delire et al., 2011; Sun & Wang, 2011; Wang et al., 2011; Zemp et al., 2017). Forest cover can degrade as a result of increasing natural disturbances such as drought and fire and/or decreasing rainfall (Verbesselt et al., 2016); on the other hand, deforestation could enhance drought through reducing evapotranspiration and weakening the atmospheric moisture supply during dry seasons (Van der Ent et al., 2010; von Randow et al., 2012). Consequently, deforestation could potentially trigger self-amplified forest loss and destabilize the forest (Wang & Eltahir, 2000a, b). However, this study prescribes vegetation cover and its changes and therefore does not account for the processes and feedback underlying a potential self-amplification of deforestation, which is a limitation that will be tackled in follow-up studies. On the other hand, even without the self-amplification effect, the magnitude of deforestation-induced local warming found in this study (2-3°C under fragmented clear cut) is alarming. This is not only because it is significantly greater than the greenhouse gas warming (which is estimated to be ~0.7 °C since 1980 in the Amazonia). More importantly, deforestation-induced warming can occur over a relatively short time when deforestation rapidly expands. The future of Amazon forest is still poorly understood due to the great uncertainties in regional climate change and the resulting forest response (Boulton et al., 2013). A large number of numerical modeling studies have pointed out the risk of Amazon forest dieback in the 21st century under the influence of climate change or in combination with human activities (Cox et al., 2000, 2004; Cochrane & Barber, 2009;Rammig et al., 2010; Boulton et al., 2013). Although these simulations are subject to a large array of uncertainties, it is rather certain that the Amazon forest will not be sustainable under current land use practices especially in an increasingly warmer climate (Boulton et al. 2017; Malhi et al. 2009).

Acknowledgment:

This research was funded by the National Science Foundation (NSF) under Grant AGS-1659953. Computing resources and data storages were provided by the NCAR Computational and Information Systems Laboratory (CISL). The authors thank the three anonymous reviewers for their constructive comments on an earlier version of this paper.

REFERENCES

Alkama, R., and A. Cescatti, 2016: Biophysical climate impacts of recent changes in global forest cover. *Science (80-.).*, **351**, 600–604.

Alves, L. M., J. A. Marengo, R. Fu, and R. J. Bombardi, 2017: Sensitivity of Amazon regional climate to deforestation. *Am. J. Clim. Chang.*, **6**, 75–98.

Badger, A. M., and P. A. Dirmeyer, 2016: Remote tropical and sub-tropical responses to Amazon deforestation. *Clim. Dyn.*, **46**, 3057–3066.

Baidya Roy, S., and R. Avissar, 2002: Impact of land use/land cover change on regional hydrometeorology in Amazonia. *J. Geophys. Res. Atmos.*, **107**, LBA-4.

Barros, V. R., J. A. Boninsegna, I. A. Camilloni, M. Chidiak, G. O. Magrín, and M. Rusticucci, 2015: Climate change in Argentina: trends, projections, impacts and adaptation. *Wiley Interdiscip. Rev. Clim. Chang.*, **6**, 151–169.

Boulton, C. A., P. Good, and T. M. Lenton, 2013: Early warning signals of simulated Amazon rainforest dieback. *Theor. Ecol.*, **6**, 373–384.

——, B. B. B. Booth, and P. Good, 2017: Exploring uncertainty of Amazon dieback in a perturbed parameter Earth system ensemble. *Glob. Chang. Biol.*, **23**, 5032–5044.

Brienen, R. J. W., and Coauthors, 2015: Long-term decline of the Amazon carbon sink. *Nature*, **519**, 344.

Cavalcante, R. B. L., P. R. M. Pontes, P. W. M. Souza-Filho, and E. B. de Souza, 2019:

Opposite Effects of Climate and Land Use Changes on the Annual Water Balance in the Amazon Arc of Deforestation. *Water Resour. Res.*,.

Chen, L., and P. A. Dirmeyer, 2019: Differing responses of the diurnal cycle of land surface and air temperatures to deforestation. *J. Clim.*, **32**, 7067–7079.

——, and ——, 2020: Reconciling the disagreement between observed and simulated temperature responses to deforestation. *Nat. Commun.*, **11**, 1–10.

Cochrane, M. A., and C. P. Barber, 2009: Climate change, human land use and future fires in the Amazon. *Glob. Chang. Biol.*, **15**, 601–612.

Cohn, A. S., N. Bhattarai, J. Campolo, O. Crompton, D. Dralle, J. Duncan, and S. Thompson, 2019: Forest loss in Brazil increases maximum temperatures within 50 km. *Environ. Res. Lett.*, **14**, https://doi.org/10.1088/1748-9326/ab31fb.

Cox, P. M., R. A. Betts, C. D. Jones, S. A. Spall, and I. J. Totterdell, 2000: Acceleration of global warming due to carbon-cycle feedbacks in a coupled climate model. *Nature*, **408**, 184.

——, R. A. Betts, M. Collins, P. P. Harris, C. Huntingford, and C. D. Jones, 2004: Amazonian forest dieback under climate-carbon cycle projections for the 21st century. *Theor. Appl. Climatol.*, **78**, 137–156.

Davidson, E. A., and Coauthors, 2012: The Amazon basin in transition. *Nature*, **481**, 321.

Dee, D. P., and Coauthors, 2011: The ERA-Interim reanalysis: Configuration and performance of the data assimilation system. *Q. J. R. Meteorol. Soc.*, **137**, 553–597.

Delire, C., N. de Noblet-Ducoudré, A. Sima, and I. Gouirand, 2011: Vegetation dynamics enhancing long-term climate variability confirmed by two models. *J. Clim.*, **24**, 2238–2257.

Duveiller, G., J. Hooker, and A. Cescatti, 2018: The mark of vegetation change on Earth's surface energy balance. *Nat. Commun.*, **9**, https://doi.org/10.1038/s41467-017-02810-8.

Eltahir, E. A. B., and R. L. Bras, 1994: Precipitation recycling in the Amazon basin. *Q. J. R. Meteorol. Soc.*, **120**, 861–880.

Van der Ent, R. J., H. H. G. Savenije, B. Schaefli, and S. C. Steele-Dunne, 2010: Origin and fate of atmospheric moisture over continents. *Water Resour. Res.*, **46**.

Erfanian, A., and G. Wang, 2018: Explicitly accounting for the role of remote oceans in regional climate modeling of South America. *J. Adv. Model. Earth Syst.*, **10**, 2408–2426.

——, ——, and L. Fomenko, 2017a: Unprecedented drought over tropical South America in 2016: significantly under-predicted by tropical SST. *Sci. Rep.*, **7**, 5811.

——, ——, ——, and M. Yu, 2017b: Ensemble-based Reconstructed Forcing (ERF) for regional climate modeling: Attaining the performance at a fraction of cost. *Geophys. Res. Lett.*, **44**, 3290–3298, https://doi.org/10.1002/2017GL073053.

Fearnside, P. M., 2005: Deforestation in Brazilian Amazonia: history, rates, and consequences. *Conserv. Biol.*, **19**, 680–688.

Feldpausch, T. R., and Coauthors, 2012: Tree height integrated into pantropical forest biomass estimates. *Biogeosciences*, 3381–3403.

Fu, R., and W. Li, 2004: The influence of the land surface on the transition from dry to wet season in Amazonia. *Theor. Appl. Climatol.*, **78**, 97–110.

Gedney, N., and P. J. Valdes, 2000: The effect of Amazonian deforestation on the northern hemisphere circulation and climate. *Geophys. Res. Lett.*, **27**, 3053–3056.

Giorgi, F., and Coauthors, 2012: RegCM4: model description and preliminary tests over multiple CORDEX domains. *Clim. Res.*, **52**, 7–29.

Hansen, M. C., Y. E. Shimabukuro, P. Potapov, and K. Pittman, 2008: Comparing annual MODIS and PRODES forest cover change data for advancing monitoring of Brazilian forest cover. *Remote Sens. Environ.*, **112**, 3784–3793.

——, and Coauthors, 2013: High-resolution global maps of 21st-century forest cover change. *Science (80-.).*, **342**, 850–853.

Hasler, N., D. Werth, and R. Avissar, 2009: Effects of tropical deforestation on global hydroclimate: A multimodel ensemble analysis. *J. Clim.*, **22**, 1124–1141.

Herold, M., and Coauthors, 2011: A review of methods to measure and monitor historical carbon emissions from forest degradation. *Unasylva*, **62**, 16–24.

Hilker, T., A. I. Lyapustin, F. G. Hall, R. Myneni, Y. Knyazikhin, Y. Wang, C. J. Tucker, and P. J. Sellers, 2015: On the measurability of change in Amazon vegetation from MODIS.

Remote Sens. Environ., **166**, 233–242.

Hirota, M., M. D. Oyama, and C. Nobre, 2011: Concurrent climate impacts of tropical South America land-cover change. *Atmos. Sci. Lett.*, **12**, 261–267.

Houghton, R. A., D. L. Skole, C. A. Nobre, J. L. Hackler, K. T. Lawrence, and W. H. Chomentowski, 2000: Annual fluxes of carbon from deforestation and regrowth in the Brazilian Amazon. *Nature*, **403**, 301.

Houspanossian, J., R. Giménez, E. Jobbágy, and M. Nosetto, 2017: Surface albedo raise in the South American Chaco: Combined effects of deforestation and agricultural changes. *Agric. For. Meteorol.*, **232**, 118–127.

Huete, A., K. Didan, T. Miura, E. P. Rodriguez, X. Gao, and L. G. Ferreira, 2002: Overview of the radiometric and biophysical performance of the MODIS vegetation indices. *Remote Sens. Environ.*, **83**, 195–213.

Hurtt, G. C., and Coauthors, 2011: Harmonization of land-use scenarios for the period 1500-2100: 600 years of global gridded annual land-use transitions, wood harvest, and resulting secondary lands. *Clim. Change*, **109**, 117–161, https://doi.org/10.1007/s10584-011-0153-2.

Imbach, P., M. Manrow, E. Barona, A. Barretto, G. Hyman, and P. Ciais, 2015: Spatial and temporal contrasts in the distribution of crops and pastures across Amazonia: A new agricultural land use data set from census data since 1950. *Global Biogeochem. Cycles*,

29, 898–916.

Khanna, J., D. Medvigy, S. Fueglistaler, and R. Walko, 2017: Regional dry-season climate changes due to three decades of Amazonian deforestation. *Nat. Clim. Chang.*, **7**, 200.

Lawrence, D., and K. Vandecar, 2015: Effects of tropical deforestation on climate and agriculture. *Nat. Clim. Chang.*, **5**, 27.

Lawrence, D. M., and Coauthors, 2011: Parameterization improvements and functional and structural advances in version 4 of the Community Land Model. *J. Adv. Model. Earth Syst.*, **3**.

Lawrence, P. J., and T. N. Chase, 2007: Representing a new MODIS consistent land surface in the Community Land Model (CLM 3.0). *J. Geophys. Res. Biogeosciences*, **112**.

Lean, J., and D. A. Warrilow, 1989: Simulation of the regional climatic impact of Amazon deforestation. *Nature*, **342**, 411.

Leite-Filho, A. T., M. H. Costa, and R. Fu, 2019: The southern Amazon rainy season: The role of deforestation and its interactions with large-scale mechanisms. *Int. J. Climatol.*,.

Lejeune, Q., E. L. Davin, B. P. Guillod, and S. I. Seneviratne, 2015: Influence of Amazonian deforestation on the future evolution of regional surface fluxes, circulation, surface temperature and precipitation. *Clim. Dyn.*, **44**, 2769–2786.

Li, W., and R. Fu, 2004: Transition of the large-scale atmospheric and land surface conditions from the dry to the wet season over Amazonia as diagnosed by the ECMWF re-analysis.

J. Clim., **17**, 2637–2651.

Li, Y., M. Zhao, S. Motesharrei, Q. Mu, E. Kalnay, and S. Li, 2015: Local cooling and warming effects of forests based on satellite observations. *Nat. Commun.*, **6**, 6603.

Liu, W., G. Wang, M. Yu, H. Chen, and Y. Jiang, 2020a: Multimodel future projections of the regional vegetation-climate system over East Asia: Comparison between two ensemble approaches. *J. Geophys. Res. Atmos.*, **125**, e2019JD031967.

——, ——, ——, ——, ——, M. Yang, and Y. Shi, 2020b: Projecting the future vegetation–climate system over East Asia and its RCP-dependence. *Clim. Dyn.*, **55**, 2725–2742, https://doi.org/10.1007/s00382-020-05411-2.

Malhi, Y., J. T. Roberts, R. A. Betts, T. J. Killeen, W. Li, and C. A. Nobre, 2008: Climate change, deforestation, and the fate of the Amazon. *Science (80-.).*, **319**, 169–172.

——, and Coauthors, 2009: Exploring the likelihood and mechanism of a climate-change-induced dieback of the Amazon rainforest. *Proc. Natl. Acad. Sci.*, **106**, 20610–20615.

Milodowski, D. T., E. T. A. Mitchard, and M. Williams, 2017: Forest loss maps from regional satellite monitoring systematically underestimate deforestation in two rapidly changing parts of the Amazon. *Environ. Res. Lett.*, **12**, 94003.

Morton, D. C., R. S. DeFries, Y. E. Shimabukuro, L. O. Anderson, F. Del Bon Espírito-Santo, M. Hansen, and M. Carroll, 2005: Rapid assessment of annual deforestation in the Brazilian Amazon using MODIS data. *Earth Interact.*, **9**, 1–22.

Nobre, C. A., and L. D. S. Borma, 2009: 'Tipping points' for the Amazon forest. *Curr. Opin. Environ. Sustain.*, **1**, 28–36.

Oleson, K. W., and Coauthors, 2013: NCAR/TN-503+STR NCAR Technical Note ___.

Patton, E. G., P. P. Sullivan, and C.-H. Moeng, 2005: The influence of idealized heterogeneity on wet and dry planetary boundary layers coupled to the land surface. *J. Atmos. Sci.*, **62**, 2078–2097.

Prodes, I. P., 2013: Monitoramento da floresta Amazônica Brasileira por satélite. *Inst. Nac. Pesqui. Espac. Proj. Prodes. Available http//www. obt. inpe. br/prodes/index. php Accessed*, **25**, 2013.

Rammig, A., and Coauthors, 2010: Estimating the risk of Amazonian forest dieback. *New Phytol.*, **187**, 694–706.

von Randow, R. C. S., C. von Randow, R. W. A. Hutjes, J. Tomasella, and B. Kruijt, 2012: Evapotranspiration of deforested areas in central and southwestern Amazonia. *Theor. Appl. Climatol.*, **109**, 205–220.

Da Rocha, H. R., and Coauthors, 2009: Patterns of water and heat flux across a biome gradient from tropical forest to savanna in Brazil. *J. Geophys. Res. Biogeosciences*, **114**.

Rochedo, P. R. R., and Coauthors, 2018: The threat of political bargaining to climate mitigation in Brazil. *Nat. Clim. Chang.*, **8**, 695.

Sampaio, G., C. Nobre, M. H. Costa, P. Satyamurty, B. S. Soares-Filho, and M. Cardoso, 2007: Regional climate change over eastern Amazonia caused by pasture and soybean cropland expansion. *Geophys. Res. Lett.*, **34**.

Satyamurty, P., C. P. W. da Costa, and A. O. Manzi, 2013: Moisture source for the Amazon Basin: a study of contrasting years. *Theor. Appl. Climatol.*, **111**, 195–209.

Schultz, N. M., P. J. Lawrence, and X. Lee, 2017: Global satellite data highlights the diurnal asymmetry of the surface temperature response to deforestation. *J. Geophys. Res. Biogeosciences*, **122**, 903–917.

Shi, Y., M. Yu, A. Erfanian, and G. Wang, 2018: Modeling the Dynamic Vegetation–Climate System over China Using a Coupled Regional Model. *J. Clim.*, **31**, 6027–6049.

Skole, D., and C. Tucker, 1993: Tropical deforestation and habitat fragmentation in the Amazon: satellite data from 1978 to 1988. *Science (80-.).*, **260**, 1905–1910.

Soares-Filho, B., R. Rajão, M. Macedo, A. Carneiro, W. Costa, M. Coe, H. Rodrigues, and A. Alencar, 2014: Cracking Brazil's forest code. *Science (80-.).*, **344**, 363–364.

Souza-Filho, P. W. M., E. B. de Souza, R. O. S. Júnior, W. R. Nascimento Jr, B. R. V. de Mendonça, J. T. F. Guimarães, R. Dall'Agnol, and J. O. Siqueira, 2016: Four decades of land-cover, land-use and hydroclimatology changes in the Itacaiúnas River watershed, southeastern Amazon. *J. Environ. Manage.*, **167**, 175–184.

Sun, S., and G. Wang, 2011: Diagnosing the equilibrium state of a coupled global biosphere-atmosphere model. *J. Geophys. Res. Atmos.*, **116**.

Swann, A. L. S., M. Longo, R. G. Knox, E. Lee, and P. R. Moorcroft, 2015: Future deforestation in the Amazon and consequences for South American climate. *Agric. For. Meteorol.*, **214**, 12–24.

Tollefson, J., 2016: Political upheaval threatens Brazil's environmental protections. *Nat. News*, **539**, 147.

Verbesselt, J., N. Umlauf, M. Hirota, M. Holmgren, E. H. Van Nes, M. Herold, A. Zeileis, and M. Scheffer, 2016: Remotely sensed resilience of tropical forests. *Nat. Clim. Chang.*, **6**, 1028.

Wang, G., and E. A. B. Eltahir, 2000: Role of vegetation dynamics in enhancing the low-frequency variability of the Sahel rainfall. *Water Resour. Res.*, **36**, 1013–1021.

——, and E. A. B. Eltahjr, 2000: Biosphere-atmosphere interactions over West Africa. I: Development and validation of a coupled dynamic model. *Q. J. R. Meteorol. Soc.*, **126**, 1239–1260.

——, S. Sun, and R. Mei, 2011: Vegetation dynamics contributes to the multi-decadal variability of precipitation in the Amazon region. *Geophys. Res. Lett.*, **38**.

——, M. Yu, J. S. Pal, R. Mei, G. B. Bonan, S. Levis, and P. E. Thornton, 2016a: On the development of a coupled regional climate–vegetation model RCM–CLM–CN–DV and its validation in Tropical Africa. *Clim. Dyn.*, **46**, 515–539.

——, ——, and Y. Xue, 2016b: Modeling the potential contribution of land cover changes to the late twentieth century Sahel drought using a regional climate model: impact of lateral boundary conditions. *Clim. Dyn.*, **47**, 3457–3477.

Wang, J., and Coauthors, 2009: Impact of deforestation in the Amazon basin on cloud climatology. *Proc. Natl. Acad. Sci.*, **106**, 3670–3674.

Yu, M., G. Wang, and J. S. Pal, 2016: Effects of vegetation feedback on future climate change over West Africa. *Clim. Dyn.*, **46**, 3669–3688.

Zemp, D. C., and Coauthors, 2017: Self-amplified Amazon forest loss due to vegetation-atmosphere feedbacks. *Nat. Commun.*, **8**, 14681.

Zeppetello, L. V., L. Parsons, J. Spector, R. Naylor, D. Battisti, Y. Masuda, and N. H. Wolff, 2020: Large scale tropical deforestation drives extreme warming. *Environ. Res. Lett.*,.

Table Captions

Table 1 Annual average for terrestrial hydrological variables (left column), and their corresponding changes

Table 2 Annual average for surface temperature variables (left column), and their corresponding changes

Table 1 Annual average for terrestrial hydrological variables (left column), and their corresponding changes. Unit for all fluxes are mm/day. W_{soil} is given in mm.

	S1_SouA	S1_BRH	S1_EastA	S2_SouA	S2_BRH	S2_EastA
ET	-0.006	0.045	-0.004	-0.015	0.052	-0.022
E_c	-0.043	0.004	-0.013	-0.042	0.005	-0.052
T_r	-0.013	0.017	-0.018	-0.041	0.026	-0.129
E_g	0.050	0.025	0.027	0.069	0.021	0.158
Precipitation	-0.104	0.046	0.001	-0.027	0.104	-0.019
W_{soil}	-0.299	-0.158	-0.114	-0.279	0.142	-0.421

Table 2 Annual average for surface temperature variables (left column), and their corresponding changes

	S1_SouA	S1_BRH	S1_EastA	S2_SouA	S2_BRH	S2_EastA
T_v	0.31	0.16	0.16	0.30	0.02	0.33
T_g	0.59	0.38	0.33	0.65	0.18	0.65
T_{2m}	0.24	0.13	0.12	0.23	0.01	0.27
T_{2m_max}	-0.10	-0.21	-0.08	-0.17	-0.23	-0.11
T_{2m_min}	0.38	0.30	0.20	0.39	0.13	0.37
T_{99}	0.19	-0.06	0.13	0.33	-0.38	0.33
F_{T99}	1.44	-0.19	0.84	2.72	-1.23	3.91

T_v, T_g, T_{2m}, T_{2m_max}, T_{2m_min}, and T_{99} are given in °C. F_{T99} is given in times/year.

Figure Captions

Figure 1. Loss of forest cover (a1-a2, in %) and the resulting annual average LAI changes (b1-b2, in m^2/m^2) and albedo changes (c1-c2).

Figure 2. Changes of the annual average ET (a1-a2), canopy evaporation (b1-b2), transpiration (c1-c2), and soil evaporation (d1-d2), in mm/day.

Figure 3. Absolute changes of the SON and annual average relative humidity (in %) at 2m above canopy (a1-a2 and b1-b2) and 800mb (c1-c2 and d1-d2).

Figure 4. Changes of the SON and annual average precipitation (a1-a2 and b1-b2, in %) and water depth in the top 10cm of soil (c1-c2 and d1-d2, in mm).

Figure 5. Correspondence between average changes of hydrological cycle variables and forest cover loss (in %) in SON, based on all grid cells with non-zero forest cover loss in the region 65-45° W, 0-30°S, for both Scenario 1 (blue) and Scenario 2 (red). a) Canopy evaporation, b) Transpiration, c) Soil evaporation, d) total ET, e) Precipitation, f) Water depth in the top 10cm of soil (in mm). Unit for all fluxes are mm/day.

Figure 6. Changes of the average vegetation temperature (a1-a4), ground temperature (b1-b4), and 2-m air temperature (c1-c4) for deforestation Scenario 1 (S1) and Scenario 2 (S2), in °C, based on annual mean and September-October-November seasonal mean.

Figure 7. Changes of daily maximum (a1-a5 and b1-b5) and minimum 2-m air temperatures (c1-c5 and d1-d5), in °C, based on the seasonal and annual means.

Figure 8. Changes of the daily average (a-c) and daily maximum (d-f) 2-m air temperatures (in °C) during the September-October-November season corresponding to forest cover loss (a and d, in %) and incident shortwave radiation (b-c and e-f, in W/m^2) for Scenario 1 (blue) and Scenario 2 (red), based on grid cell with forest cover loss (a-b, d-f) and those without (c, f) within the region 65-45° W, 0-30°S.

Figure 9. Changes of the annual mean fluxes of incident shortwave radiation (a1-a2), emitted longwave radiation (b1-b2), R_{net} (c1-c2), latent heat flux (d1-d2) and sensible heat (e1-e2), in W/m^2.

Figure 10. Changes to the 99th percentile of the average 2-m air temperature (a1-a2, in °C) and changes to the number of days with temperature exceeding the 99th percentile (b1-b2, in days/year).

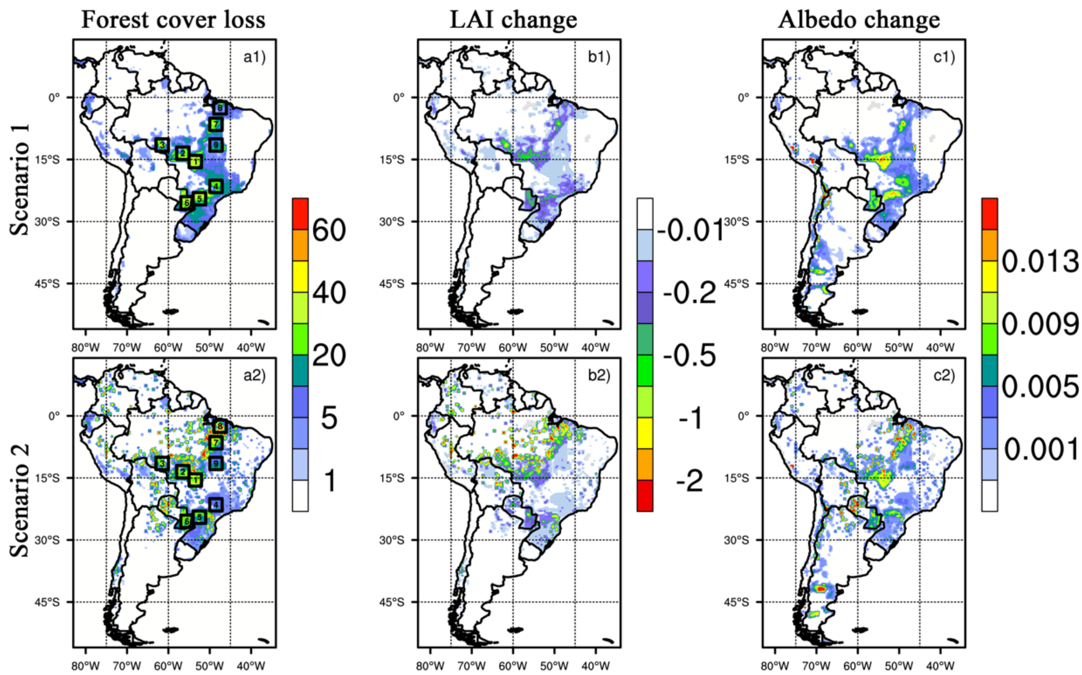

777

778 **Figure 1.** Loss of forest cover (a1-a2, in %) and the resulting annual average LAI changes (b1-b2, in
779 m^2/m^2) and albedo changes (c1-c2).

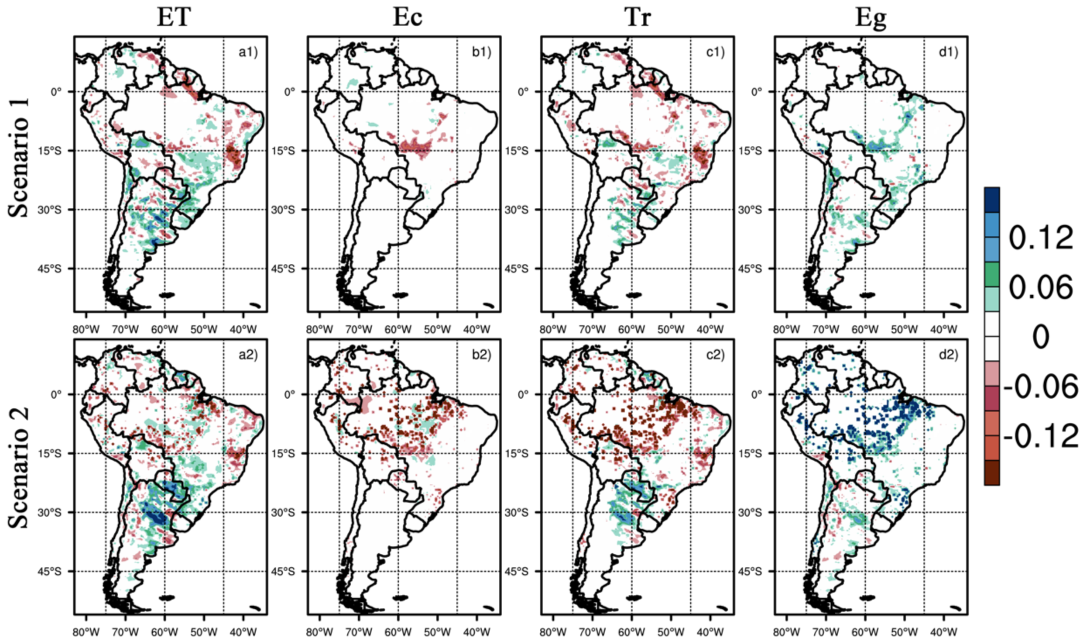

Figure 2. Changes of the annual average ET (a1-a2), canopy evaporation (b1-b2), transpiration (c1-c2), and soil evaporation (d1-d2), in mm/day.

783

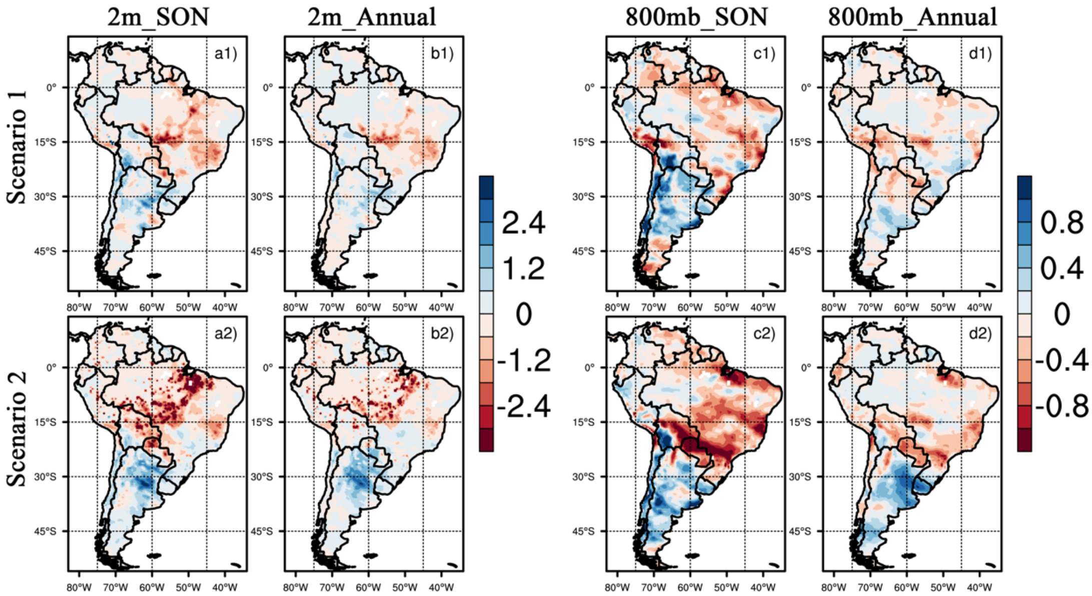

784 **Figure 3.** Absolute changes of the SON and annual average relative humidity (in %) at 2m above

785 canopy (a1-a2 and b1-b2) and 800mb (c1-c2 and d1-d2).

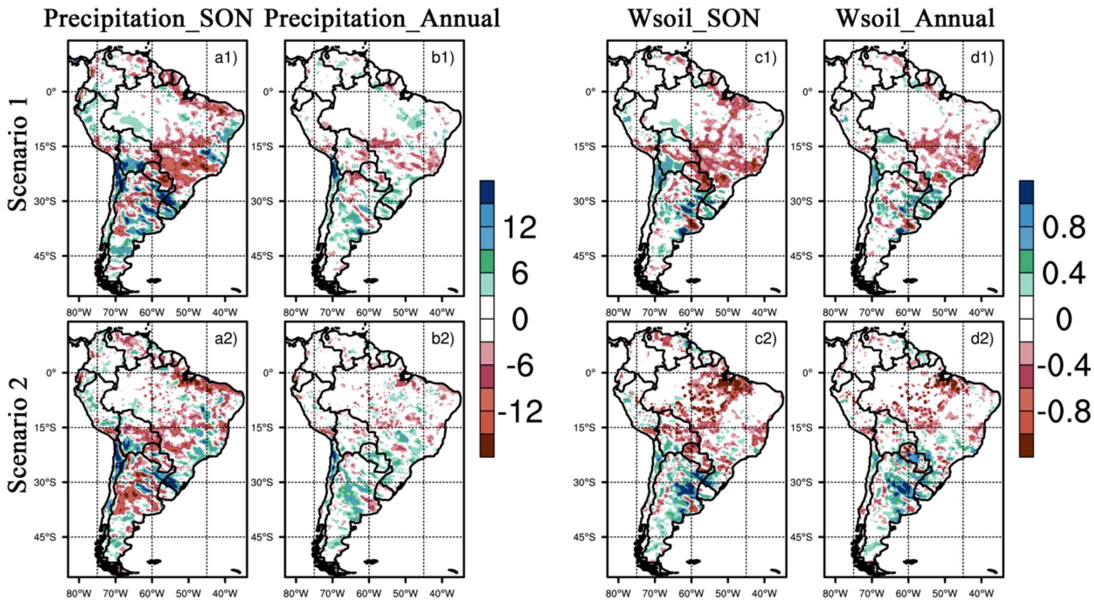

786

787 **Figure 4.** Changes of the SON and annual average precipitation (a1-a2 and b1-b2, in %) and water depth in the top 10cm of soil (c1-c2 and d1-d2, in mm).

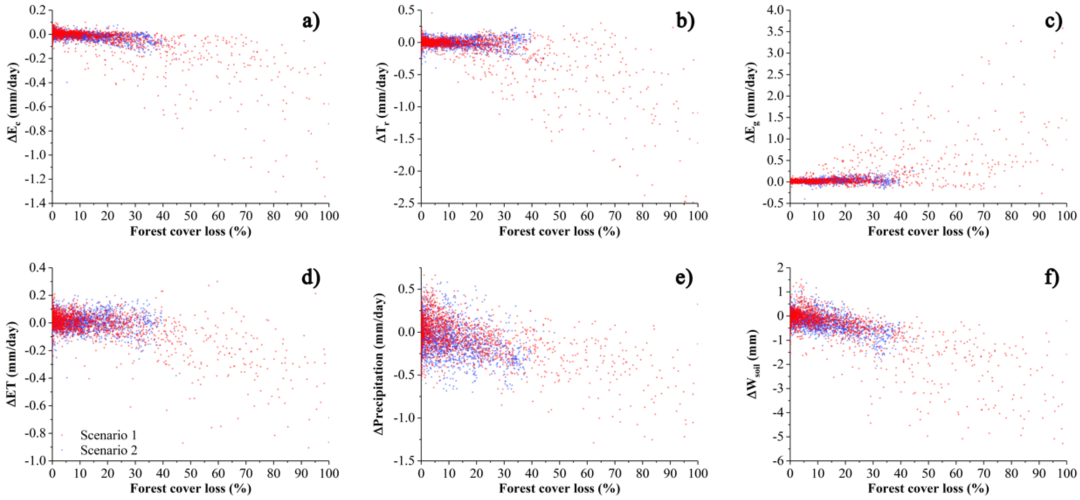

Figure 5. Correspondence between average changes of hydrological cycle variables and forest cover loss (in %) in SON, based on all grid cells with non-zero forest cover loss in the region 65-45° W, 0-30°S, for both Scenario 1 (blue) and Scenario 2 (red). a) Canopy evaporation, b) Transpiration, c) Soil evaporation, d) total ET, e) Precipitation, f) Water depth in the top 10cm of soil (in mm). Unit for all fluxes are mm/day.

796

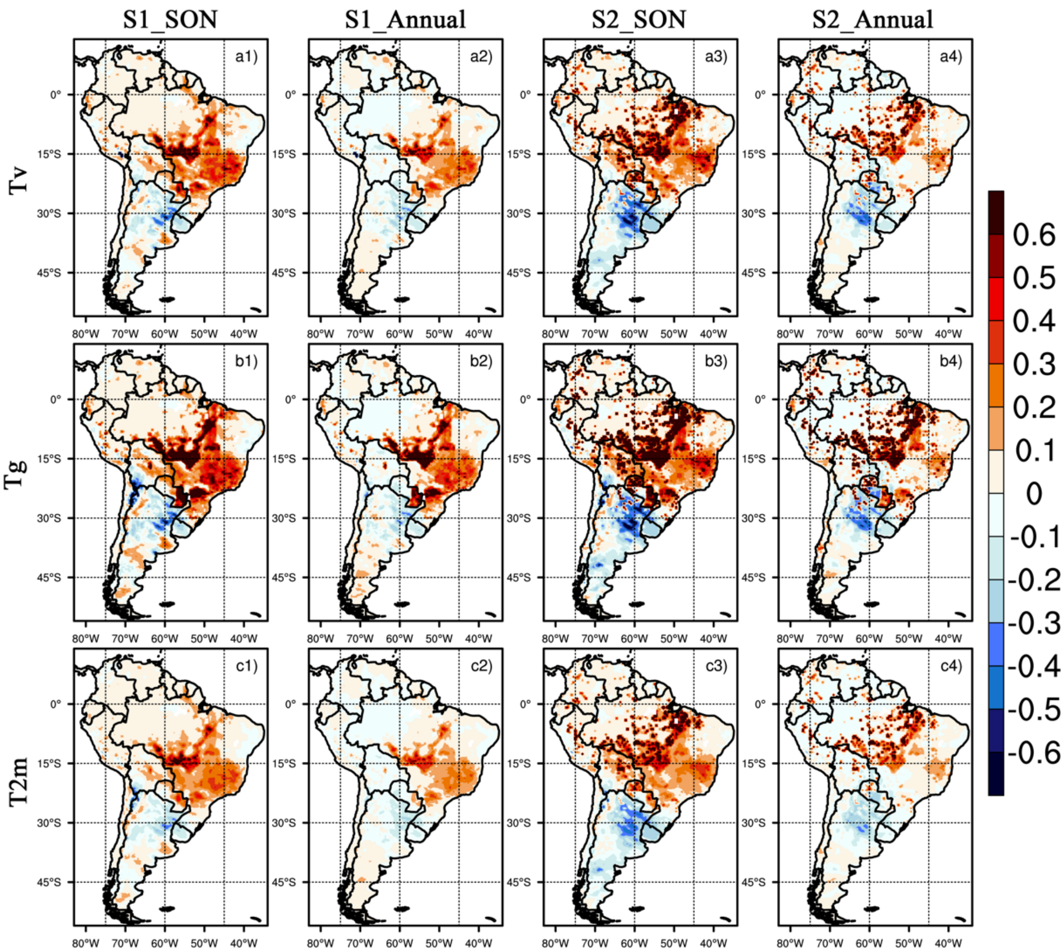

797 **Figure 6.** Changes of the average vegetation temperature (a1-a4), ground temperature (b1-b4), and
798 2-m air temperature (c1-c4) for deforestation Scenario 1 (S1) and Scenario 2 (S2), in °C, based on
799 annual mean and September-October-November seasonal mean.

800

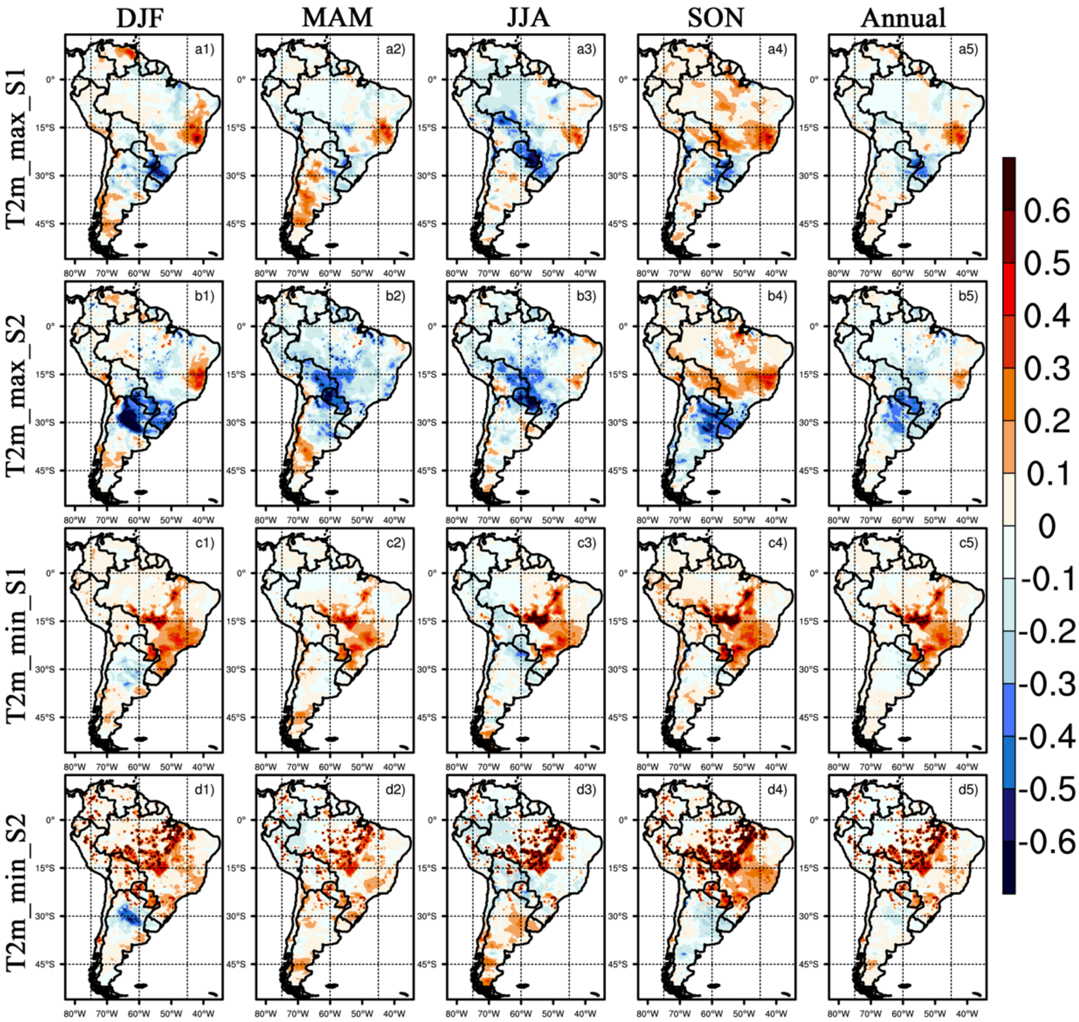

Figure 7. Changes of daily maximum (a1-a5 and b1-b5) and minimum 2-m air temperatures (c1-c5 and d1-d5), in °C, based on the seasonal and annual means.

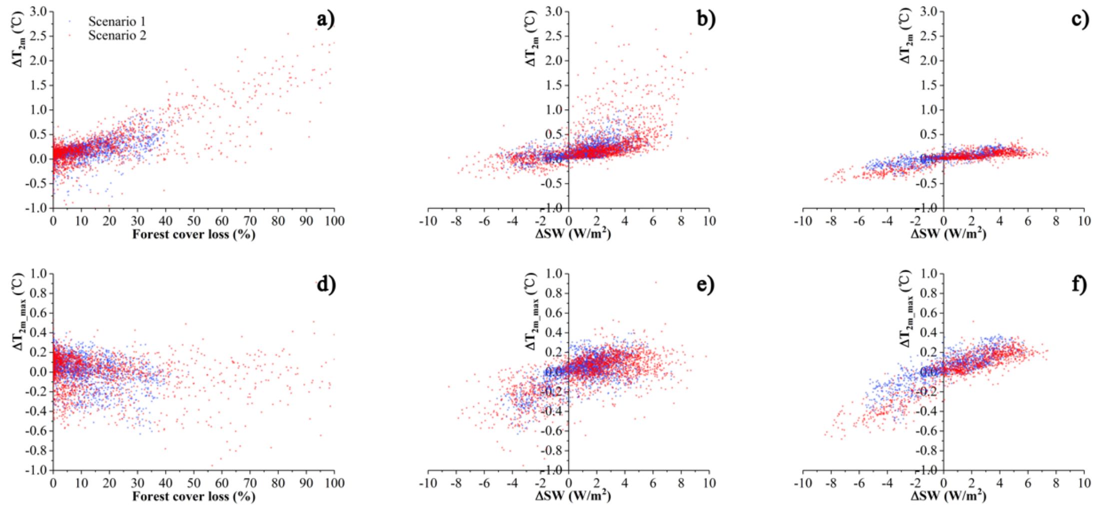

Figure 8. Changes of the daily average (a-c) and day-time maximum (d-f) 2-m air temperatures (in °C) during the September-October-November season corresponding to forest cover loss (a and d, in %) and incident shortwave radiation (b-c and e-f, in W/m^2) for Scenario 1 (blue) and Scenario 2 (red), based on grid cell with forest cover loss (a-b, d-f) and those without (c, f) within the region 65-45° W, 0-30°S.

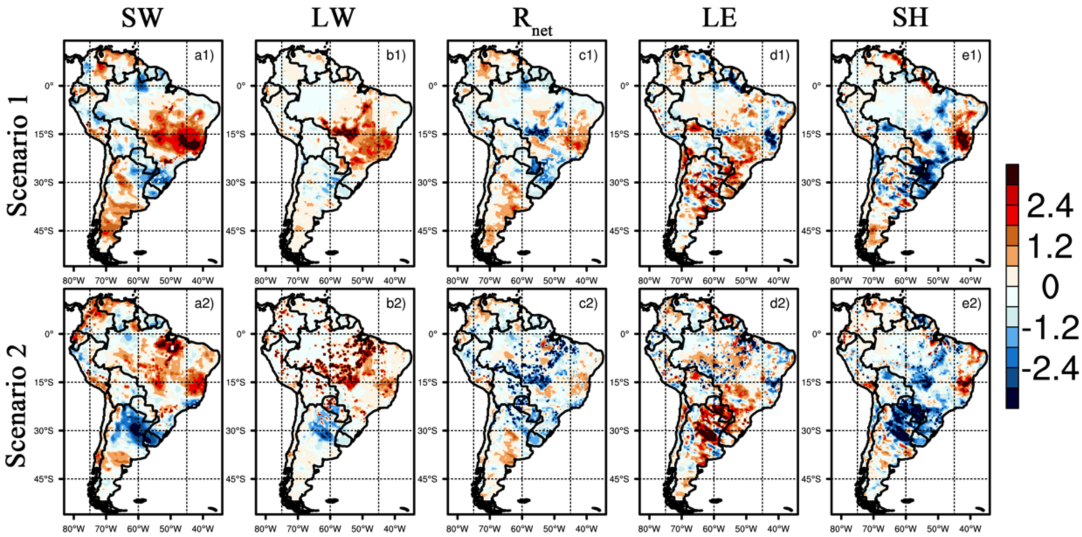

Figure 9. Changes of the annual mean fluxes of incident shortwave radiation (a1-a2), emitted longwave radiation (b1-b2), R_{net} (c1-c2), latent heat flux (d1-d2) and sensible heat (e1-e2), in W/m^2.

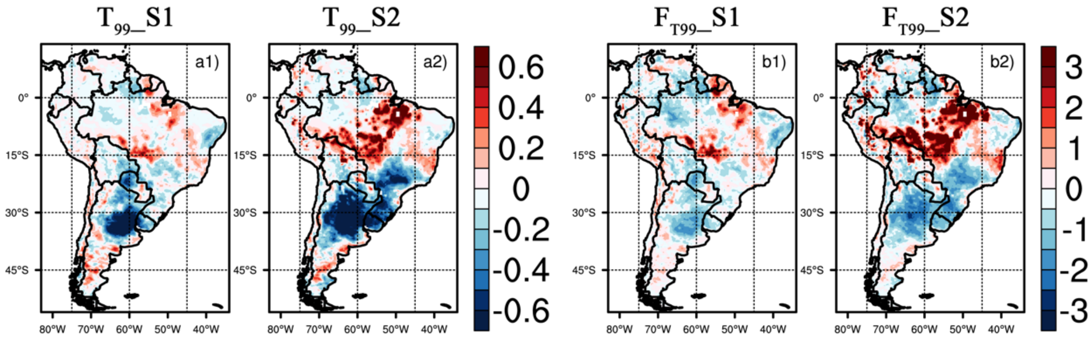

Figure 10. Changes to the 99th percentile of the average 2-m air temperature (a1-a2, in °C) and changes to the number of days with temperature exceeding the 99th percentile (b1-b2, in days/year).